Visualization of the microcirculatory network in skin by high frequency optoacoustic mesoscopy

Mathias Schwarz,[1] Juan Aguirre,[1] Andreas Buehler,[1] Murad Omar,[1] Vasilis Ntziachristos[1]
[1]Chair for Biological Imaging, Technische Universität München and Helmholtz Zentrum München, German Research Center for Environment and Health, Institute for Biological and Medical Imaging, Ingolstädter Landstraße 1, 85764 Neuherberg, Germany

ABSTRACT

Optoacoustic (photoacoustic) imaging has a high potential for imaging melanin-rich structures in skin and the microvasculature of the dermis due to the natural chromophores (de)oxyhemoglobin, and melanin. The vascular network in human dermis comprises a large network of arterioles, capillaries, and venules, ranging from 5 μm to more than 100 μm in diameter. The frequency spectrum of the microcirculatory network in human skin is intrinsically broadband, due to the large variety in size of absorbers. In our group we have developed raster-scan optoacoustic mesoscopy (RSOM) that applies a 100 MHz transducer with ultra-wide bandwidth in raster-scan mode achieving lateral resolution of 18 μm. In this study, we applied high frequency RSOM to imaging human skin in a healthy volunteer. We analyzed the frequency spectrum of anatomical structures with respect to depth and show that frequencies >60 MHz contain valuable information of structures in the epidermis and the microvasculature of the papillary dermis. We illustrate that RSOM is capable of visualizing the fine vascular network at and beneath the epidermal-dermal junction, revealing the vascular fingerprint of glabrous skin, as well as the larger venules deeper inside the dermis. We evaluate the ability of the RSOM system in measuring epidermal thickness in both hairy and glabrous skin. Finally, we showcase the capability of RSOM in visualizing benign nevi that will potentially help in imaging the penetration depth of melanoma.

Keywords: mesoscopy, microcirculation, optoacoustic, photoacoustic, skin, frequency analysis

1. INTRODUCTION

Blood vessels in human dermis range from 5 μm thick capillaries [1] to larger venules measuring up to 100 μm in diameter, which are located deeper inside the dermis [2]. Thus, the optoacoustic frequency spectrum generated by the vascular network of human dermis is intrinsically broadband. The microvascular network is affected by several skin diseases, such as systemic sclerosis [3, 4], psoriasis [5], burns, and wounds. Meanwhile, the penetration depth is a significant factor in the staging of melanoma skin cancer, which helps in the prognosis of recurrence after excision[6-8]. Invasion beyond the basement membrane located between the epidermis and dermis plays an important role in tumor invasion [9]. In many instances it would be ideal to be able to determine the depth of a lesion or to determine changes in the superficial microvasculature or deeper-seated arteriovenous networks in skin diseases as it can better outline an optimal therapeutic strategy.

Photoacoustic microscopy using a transducer with 50 MHz central frequency has been applied to skin imaging. [10-12]. The photoacoustic system applied in these experiments has a lateral resolution of >45 μm, which has been identified as limitation of photoacoustic microscopy in visualizing the microcirculatory network of the papillary dermis [13]. Thus, the *stratum corneum* in thin skin and the fine microvasculature with tube diameters of 15 μm and less could not well be visualized. Setups different from single transducer raster-scans have been used as well to image human skin. For example a linear array of detectors at 25.4 MHz central frequency has been used to measure tissue burn and superficial skin lesions several millimeters deep in tissue [14]. To improve upon the resolution of the linear array setup a bi-directional scanning approach has been applied providing quasi-isotropic lateral resolution of <100 μm [15]. Recently, human skin was imaged using an ultrasonic transducer with 100 MHz central frequency, allowing the visualization of small microvascular structures in the dermal papillae as well as larger vessels situated in the horizontal plexus of the dermis [16, 17]. With the same raster-scan system angiogenesis in microvessels around melanoma tumor has been shown [18].

Opto-Acoustic Methods and Applications in Biophotonics II, edited by Vasilis Ntziachristos, Roger Zemp,
Proc. of SPIE Vol. 9539, 95390J · © 2015 SPIE · CCC code: 1605-7422/15/$18 · doi: 10.1117/12.2183463

Here, we present skin images taken with a raster-scan mesoscopy system (RSOM) applying a transducer of 100 MHz central frequency recently built in our lab [19]. We demonstrate the importance of frequencies above 60 MHz in skin imaging by analyzing the contribution of different frequencies with respect to anatomical structures of the dermis. We further show the capability of our system to visualize the *stratum corneum* in both glabrous and hairy skin, which allows determining the width of the epidermis. Finally, we image a benign nevus, and show the potential of RSOM in melanoma screening.

2. METHODS AND MATERIALS

In the RSOM system we utilized an ultra-wideband transducer at 100 MHz central frequency with an f-number of ~1 that was connected to a 63dB amplifier (AU-1291, MITEQ Inc.). Data were acquired at an acquisition rate of 1 GS/s. The tissue was excited by <1 ns pulses, operating at 532 nm and up to 2 kHz. The laser energy per pulse was chosen according to scanning speed and illuminated skin surface. Laser energy was maintained under the laser safety limit of 20 mJ/cm^2 per pulse [20] as well as the maximum permissible pulse repetition frequency, in case of repetitive pulsing for less than 10 s [11]. Two piezo-electric positioning stages were used to raster-scan the transducer over the sample with a step size of 10 µm.

We designed a custom-made hand holder to reduce motion artifacts. The holder had an opening in the middle to allow direct contact of human skin with water used as coupling material. We imaged a region of 8 mm x 8 mm. The acquisition time was approximately 5.3 minutes for the whole area.

Taking into account the directivity of the focused transducer, a beam-forming reconstruction method based on back-projection was used [19, 21]. The reconstruction grid was set to 3 µm x 10 µm × 10 µm. Before reconstruction the raw data was bandpass filtered, which allowed us to analyze the frequency spectrum of anatomical structures within certain frequency bands. In the final images reconstructions at different frequency bands are overlain in different colors in order to emphasize high-frequency structures.

To improve visibility of vessels a vessel filter was applied to Fig. 3(d,e) [22].

To evaluate the performance of RSOM in human skin, four different areas on the arm of a healthy volunteer have been imaged. The finger pad of the thumb, and the thenar were chosen as an example of glabrous skin, which features a thick epidermal layer and epidermal ridges. The dorsum of hand between metacarpal I and II is exemplary for hairy skin, which features a much thinner epidermal layer. The fourth region comprised a benign nevus located on the lower arm.

3. RESULTS

To analyze the frequency spectrum of different anatomical structures in the human palm we bandpass filtered the raw data at different frequency bands before reconstruction. Fig. 1 shows how the anatomical structures of cross-sectional cuts through the skin depend on the frequency range employed in the reconstruction. In the frequency range between 2 - 20 MHz, shown in Fig. 1(a), the *stratum corneum* is not visible and most structures in the subpapillary plexus disappear. Deeper seated vessels located at a depth of 1 - 1.5 mm display at low resolution. The frequency band between 20 - 60 MHz, shown in Fig. 1(b), holds information on the *stratum corneum,* and finer structures in the papillary dermis. The width of the epidermal layer is clearly visible. Vessels below the papillary dermis at around 1 mm depth are still seen. The frequency band from 60 - 180 MHz, shown in Fig. 1(c), contains detailed information on the *stratum corneum* and fine structures in the zone of dermal papillae as well as the upper subpapillary plexus. To enhance the contrast of high frequency components we overlaid images reconstructed at different frequencies in Fig. 1(e). Compared to Fig. 1(d), where we reconstructed a cross section over the whole frequency range, the overlay enriches small anatomical structures located in the papillary dermis. The overlay enables to display large vascular structures in the low frequency range captured from lower parts of the dermis with fine structures at high frequencies located in the subpapillary plexus and the *stratum corneum* in the same image.

To show the capability of the applied high frequency system to visualize the width of the epidermis we performed scans of hairy skin at the back of the hand, and of glabrous skin at the thumb tip and the thenar area, as shown in Fig. 2(a-c). Cross-sectional cuts through the reconstructed volume at the three locations of interest are shown in Fig. 2(d-f).

Independent of location the *stratum corneum*, i.e. the upper layer of the epidermis, is clearly visible. We measured the vertical distance of the skin surface to the first vessels in the papillary dermis to determine the width of the epidermal layer. The width of the epidermis varies strongly between different locations. The thickness of thin skin at the back of the hand measured ~70 μm, the epidermis at the palm measured ~190 μm and the thickness at the finger measured ~310 μm.

To show that the high frequency system applied in this work is capable of visualizing fine structures in the epidermis, dermal papillae, and the vessel network in the papillary and upper reticular dermis we analyzed horizontal layers of human skin. Fig. 3(a) shows a cross-sectional slice through the ROI as well as the different skin layers that we observed with RSOM. Fig. 3(b-e) show maximum amplitude projections (MAPs) in depth direction of horizontal layers at different depths. The skin surface in Fig. 3(b) shows up as a homogeneous surface. The intensity is decreased in the center because of dark-field illumination in this area. The epidermal-dermal junction is depicted in Fig. 3(c). We observe stripes in this region that are separated by ~ 0.9 mm, which corresponds to the spacing of the friction ridges of the skin in this region [23]. Fig. 3(d) depicts the vessel network of the dermis, below the dermal papillae. Beneath the network of small vessels, we observe larger vessels deeper inside the dermis.

Fig. 4 depicts the image of a benign nevus that was acquired with RSOM. The high frequency band, encoded by the cyan color map, shows strong signal on the skin surface and the upper microvascular structures of the dermis. Frequencies below 60 MHz, encoded by the red channel in Fig. 4, hold information on the skin surface as well as the vascular network of larger vessels to a depth of ~ 1 mm. Comparing Fig. 4(a) with Fig. 4(b), we observe a strong contrast of the benign nevus with respect to the surrounding absorbers in the epidermis. The vascular network below the mole is not affected, as shown in Fig. 4(c). Fig. 4(d) shows the reconstructed optoacoustic image as can be seen from the side, revealing the superficiality of the nevus.

4. DISCUSSION AND CONCLUSION

We have imaged healthy human skin with an optoacoustic mesoscopy system at high frequencies and analyzed the frequency spectrum of different structures in skin. Our broadband transducer allowed us to reconstruct optoacoustic images at different frequency ranges from 10 - 180 MHz. We have shown that high ultrasonic frequencies above 60 MHz contain important information on the structure of the *stratum corneum* and the microvessels of the papillary dermis, which is explained by the fact that structures in this regime are in the range of 10 μm and, thus, produce optoacoustic frequencies around and above 100 MHz.

The size of anatomical structures resolved in RSOM images slowly increases with depth. The decrease in resolution with depth may be attributed partly to ultrasound attenuation that is stronger for high frequencies. Since anatomically vessels tend to increase in size the deeper they are located in skin, this is not a limitation of optoacoustics [24, 25].

In different location on the body we were able to image the skin surface and the microvessels beneath the epidermal-dermal junction of both hairy and glabrous skin. Thus, we were capable of measuring the epidermal thickness. Furthermore, we show the strong contrast of benign nevi due to melanin in our images, which shows the prospect of revealing infiltration of melanoma with RSOM.

Since the resolution of the raster-scan system presented herein has an axial resolution of 4 μm, the quality of the images is affected by motion in *in vivo* experiments. Due to motion artifacts, the microvasculature in the upper dermis appears disrupted. Motion reduction and motion compensation will be the work of future studies. Nonetheless, this study illustrates that for the visualization of the small vasculature of the upper dermis, frequencies > 60 MHz are required.

5. ACKNOWLEDGEMENTS

Andreas Buehler and Vasilis Ntziachristos acknowledge funding from the European Union project FAMOS (FP7 ICT, contract no. 317744). Juan Aguirre acknowledges funding from the European Marie Curie IEF fellowships, project HIFI.

REFERENCES

[1] A. Yen, and I. M. Braverman, "Ultrastructure of the human dermal microcirculation: the horizontal plexus of the papillary dermis," J Invest Dermatol, 66(3), 131-42 (1976).

[2] I. M. Braverman, "The cutaneous microcirculation: ultrastructure and microanatomical organization," Microcirculation, 4(3), 329-40 (1997).

[3] F. M. Wigley, "Vascular Disease in Scleroderma," Clinical Reviews in Allergy & Immunology, 36(2-3), 150-175 (2009).

[4] A. L. Herrick, "Vascular function in systemic sclerosis," Curr Opin Rheumatol, 12(6), 527-33 (2000).

[5] R. Archid, A. Patzelt, B. Lange-Asschenfeldt *et al.*, "Confocal laser-scanning microscopy of capillaries in normal and psoriatic skin," J Biomed Opt, 17(10), 101511 (2012).

[6] W. H. Clark, Jr., L. From, E. A. Bernardino *et al.*, "The histogenesis and biologic behavior of primary human malignant melanomas of the skin," Cancer Res, 29(3), 705-27 (1969).

[7] A. Breslow, "Thickness, cross-sectional areas and depth of invasion in the prognosis of cutaneous melanoma," Ann Surg, 172(5), 902-8 (1970).

[8] C. Garbe, P. Buttner, J. Bertz *et al.*, "Primary cutaneous melanoma. Identification of prognostic groups and estimation of individual prognosis for 5093 patients," Cancer, 75(10), 2484-91 (1995).

[9] I. Moll, [Duale Reihe Dermatologie] Georg Thieme Verlag, 3-14 (2010).

[10] H. F. Zhang, K. Maslov, G. Stoica *et al.*, "Functional photoacoustic microscopy for high-resolution and noninvasive in vivo imaging," Nat Biotechnol, 24(7), 848-51 (2006).

[11] H. F. Zhang, K. Maslov, and L. V. Wang, "In vivo imaging of subcutaneous structures using functional photoacoustic microscopy," Nat Protoc, 2(4), 797-804 (2007).

[12] C. P. Favazza, O. Jassim, L. A. Cornelius *et al.*, "In vivo photoacoustic microscopy of human cutaneous microvasculature and a nevus," J Biomed Opt, 16(1), 016015 (2011).

[13] J. Enfield, E. Jonathan, and M. Leahy, "In vivo imaging of the microcirculation of the volar forearm using correlation mapping optical coherence tomography (cmOCT)," Biomed Opt Express, 2(5), 1184-93 (2011).

[14] L. Vionnet, J. Gateau, M. Schwarz *et al.*, "24MHz Scanner for Optoacoustic Imaging of Skin and Burn," IEEE Trans Med Imaging, (2013).

[15] M. Schwarz, A. Buehler, and V. Ntziachristos, "Isotropic high resolution optoacoustic imaging with linear detector arrays in bi-directional scanning," J Biophotonics, 9999(9999), (2014).

[16] J. Aguirre, M. Schwarz, D. Soliman *et al.*, "Broadband mesoscopic optoacoustic tomography reveals skin layers," Optics Letters, 39(21), 6297 (2014).

[17] M. Schwarz, M. Omar, A. Buehler *et al.*, "Implications of Ultrasound Frequency in Optoacoustic Mesoscopy of the Skin," IEEE Trans Med Imaging, (2014).

[18] M. Omar, M. Schwarz, D. Soliman *et al.*, "Pushing the Optical Imaging Limits of Cancer with Multi-Frequency-Band Raster-Scan Optoacoustic Mesoscopy (RSOM)," Neoplasia, 17(2), 208-14 (2015).

[19] M. Omar, D. Soliman, J. Gateau *et al.*, "Ultrawideband reflection-mode optoacoustic mesoscopy," Opt Lett, 39(13), 3911-4 (2014).

[20] American National Standards Institute, and The Laser Institute of America, [American National Standard for safe use of lasers : approved March 16, 2007] The Laser Institute of America, Orlando, FLa.(2007).

[21] M. Omar, J. Gateau, and V. Ntziachristos, "Raster-scan optoacoustic mesoscopy in the 25-125 MHz range," Opt Lett, 38(14), 2472-4 (2013).

[22] A. F. Frangi, W. J. Niessen, K. L. Vincken *et al.*, "Multiscale vessel enhancement filtering," Medical Image Computing and Computer-Assisted Intervention - Miccai'98, 1496, 130-137 (1998).

[23] G. J. Liu, and Z. P. Chen, "Capturing the vital vascular fingerprint with optical coherence tomography," Applied Optics, 52(22), 5473-5477 (2013).

[24] I. M. Braverman, and A. Keh-Yen, "Ultrastructure of the human dermal microcirculation. III. The vessels in the mid- and lower dermis and subcutaneous fat," J Invest Dermatol, 77(3), 297-304 (1981).

[25] I. M. Braverman, and A. Yen, "Ultrastructure of the human dermal microcirculation. II. The capillary loops of the dermal papillae," J Invest Dermatol, 68(1), 44-52 (1977).

FIGURES

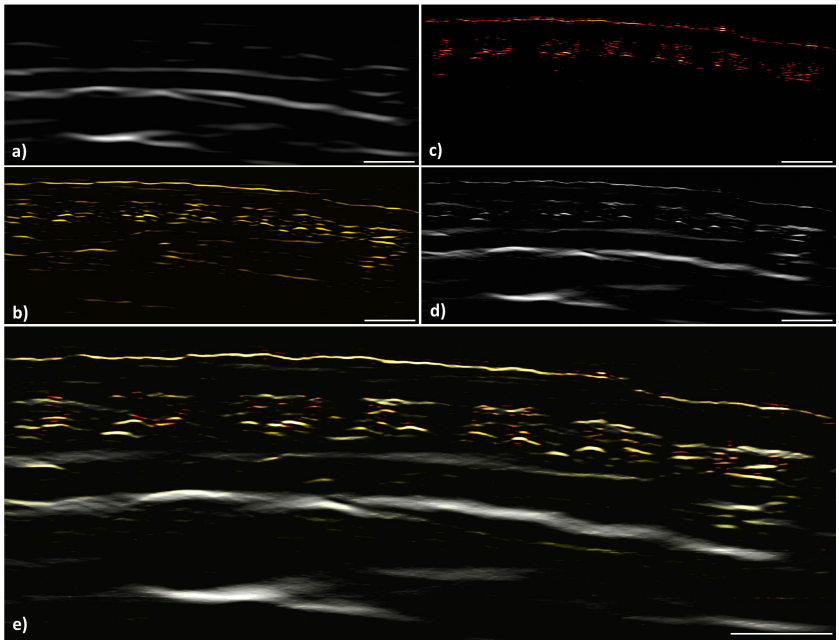

Fig. 1: Frequency content in human skin. Cross-sectional cut through the reconstructed image of a palm at different frequency bands: a) Reconstruction bandwidth 2-20 MHz. b) Reconstruction bandwidth 20-60 MHz. c) Reconstruction bandwidth 60-180 MHz. d) Reconstruction bandwidth 2-180 MHz. e) Overlay of reconstructions at various bandwidths: white (2-180 MHz), yellow (20-180 MHz) and red (60-180 MHz). All scale bars: 500 µm

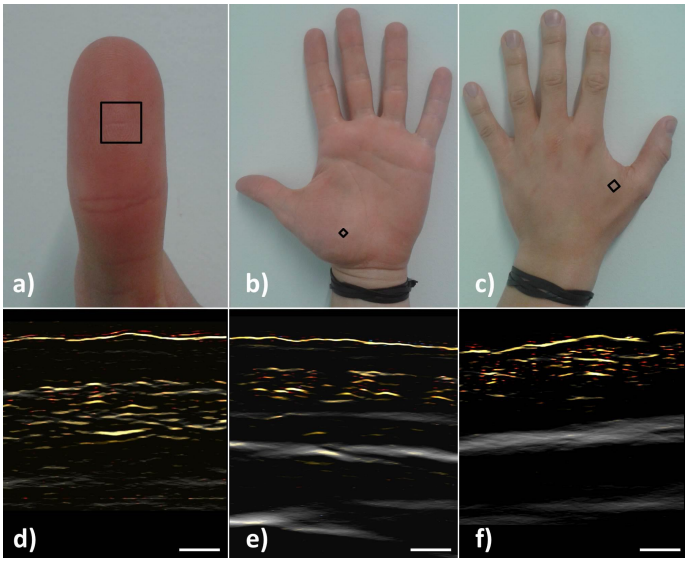

Fig. 2: Epidermal thickness of skin at different locations. The locations marked in a), b), and c) correspond to the reconstructed cross-sectional slices depicted in d), e) and f), respectively. d) Glabrous skin located at the thumb tip. e) Glabrous skin located at the palm close to the thumb. f) Hairy skin located at the hand wrist close to the thumb. All scale bars: 250 µm

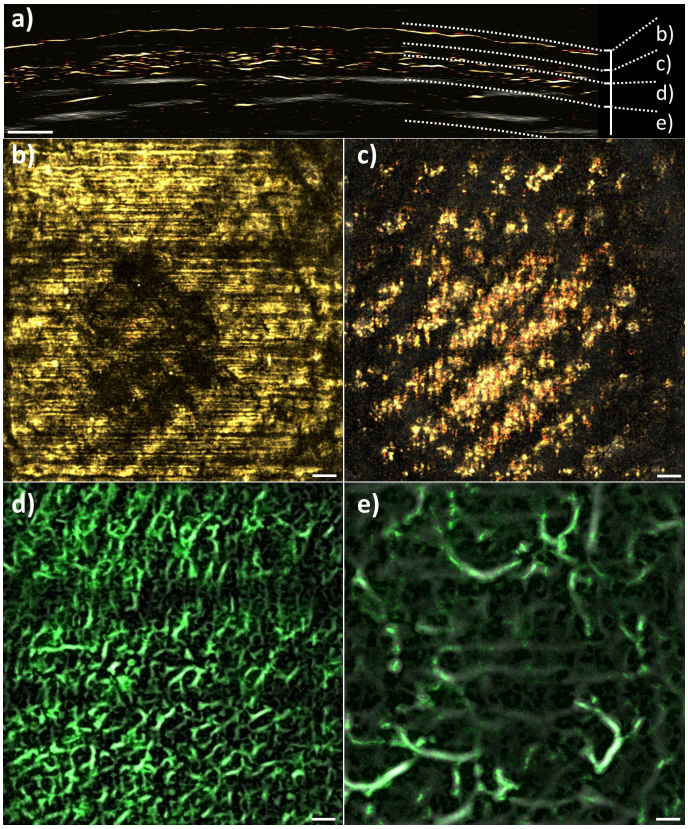

Fig. 3: Layers of human skin. a) Reconstructed cross-sectional cut through human skin. (b-e) Maximum amplitude projections along the depth direction within the layers marked in (a). b) Epidermis, c) Dermal papillae, d) Upper papillary dermis, e) Deep papillary dermis and upper reticular dermis. In (d,e) the original image (green) is overlain with an image filtered for vessels in white. All scale bars: 500 µm

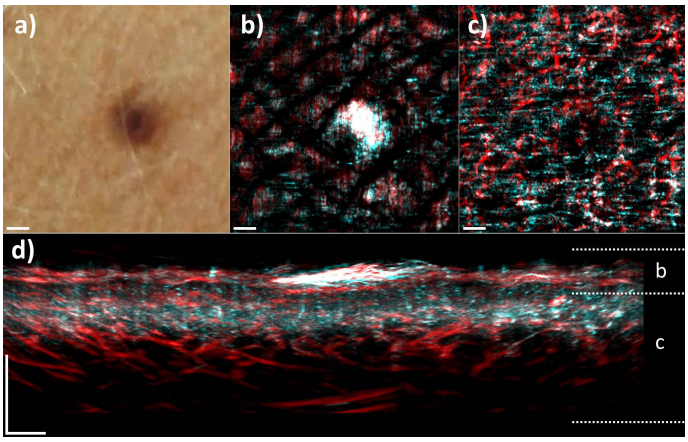

Fig. 4. Visualization of a benign nevus. a) ROI containing a melanin-rich mole. b) MAP of upper layer of the ROI shown in (a). c) MAP of the vascular network below the mole shown in (b). The depth range of the MAPs in (b), and (c) is shown in (d), respectively. d) Side-view of the 3-D volume acquired by scanning the ROI shown in (a). The red channel shows frequencies between 20-60 MHz, The cyan channel shows frequencies between 60-180 MHz. All scale bars: 500 µm